FABRICATION OF LUMINESCENT CELLULOSE-BASED PARTICLES FROM SUGARCANE BAGASSE FOR Fe^{3+} DETECTION

BERLIAN SITORUS,[*] MAHADI,[*] RISYA SASRI,[*] DIONISIUS RIO,[*]
INTAN SYAHBANU[*] and SENO D. PANJAITAN[**]

[*]*Department of Chemistry, Universitas Tanjungpura,*
Jl. Prof. Dr. H. Hadari Nawawi, Pontianak 78124, West Kalimantan, Indonesia
[**]*Department of Electrical Engineering, Universitas Tanjungpura,*
Jl. Prof. Dr. H. Hadari Nawawi, Pontianak 78124, West Kalimantan, Indonesia
✉ *Corresponding author: B. Sitorus, berlian.sitorus@chemistry.untan.ac.id*

Received July 10, 2025

This study reports on the synthesis of luminescent nanoparticles (LNPs) derived from sugarcane bagasse, offering a sustainable approach for detecting Fe^{3+} ions in aqueous systems. The process began with the isolation of cellulose through alkali and bleaching treatments, followed by acid hydrolysis to produce nanocellulose. Subsequent hydrothermal carbonization at 200 °C for 12 h yielded a reddish-brown colloidal suspension. Characterization by UV-Vis spectroscopy revealed a prominent absorption band at 284 nm, while particle size analysis indicated an average diameter of 192.7 nm. FT-IR spectra confirmed chemical modifications consistent with carbonization. Photoluminescence measurements showed a strong blue emission at ~445 nm, which decreased steadily with rising Fe^{3+} concentrations from 0.1 to 100 μM, consistent with a dynamic quenching mechanism. These findings demonstrate that the synthesized LNPs retain nanoscale features and exhibit optical sensitivity toward Fe^{3+} ions, suggesting their potential use as simple, eco-friendly fluorescence-based sensors for heavy metal detection. It was concluded that luminescent nanoparticles can be applied as a detector of heavy metals (Fe^{3+}).

Keywords: Fe^{3+} detection, luminescent nanoparticles, nanocellulose, sugarcane bagasse

INTRODUCTION

Cellulose, a structurally robust and renewable polysaccharide, is the most abundant biopolymer on Earth and continues to attract significant scientific interest for its applications in materials science, environmental remediation, and biomedical technology. Its β-1,4-glycosidic-linked glucose backbone forms microfibrillar structures with high tensile strength, chemical modifiability, and biocompatibility.[1-3] Among various lignocellulosic resources, sugarcane bagasse, a low-cost byproduct of sugar production, presents a valuable source of cellulose that can be isolated through conventional delignification and purification processes.[4,5]

The chemical structure of cellulose, particularly the abundance of hydroxyl and carbonyl functional groups, enables interactions with various pollutants and metal ions *via* adsorption, ion exchange, or surface complexation mechanisms.[6] These properties can be enhanced through further modification or processing into colloidal and nanoscale structures. In particular, cellulose-based particles have shown potential as luminescent materials, opening opportunities in fluorescence sensing due to their low toxicity, aqueous stability, and functional responsiveness.

Fluorescence-based sensors offer notable advantages, including high sensitivity, fast response, and compatibility with portable detection systems. These features are especially valuable for monitoring hazardous ions such as Fe^{3+}, which is prevalent in natural and industrial waters and poses health risks at elevated levels.[7]

Conventional detection methods, such as ICP-MS and AAS, provide excellent precision, but are expensive, require complex instrumentation, and

necessitate skilled operators. In contrast, luminescent sensors, particularly those utilizing organic dyes, quantum dots, and other similar technologies, offer attractive advantages, including high sensitivity, simplicity, and the potential for real-time monitoring.[8]

Luminescent cellulose particles, particularly those derived from lignocellulosic waste, represent a promising alternative for developing responsive fluorescence sensors.[9] However, reports on the fabrication of luminescent cellulose materials from sugarcane bagasse for metal ion detection remain scarce.

This study presents a green synthesis of luminescent nanoparticles directly from purified cellulose extracted from sugarcane bagasse, without requiring any additional dopants or passivators, and demonstrates their application in aqueous Fe^{3+} sensing, thus offering a sustainable and low-cost alternative to conventional routes. By converting agricultural waste into functional materials with optical sensing capabilities, this work advances biomass utilization strategies while addressing critical needs in environmental monitoring.

EXPERIMENTAL

Materials

Sugarcane bagasse, collected from a local sugarcane juice vendor in Pontianak City, Indonesia, was used as the primary cellulose source. The materials included distilled water, ethanol (95–97%), filter paper, sulfuric acid (H_2SO_4), sodium hydroxide (NaOH), sodium hypochlorite (NaOCl, 12%), and sodium bicarbonate ($NaHCO_3$). Commercial cellulose was used as a reference material. All chemicals were of analytical grade and, unless otherwise stated, were purchased from Merck.

Pretreatment of sugarcane bagasse

The fabrication steps of luminescent cellulose-based particles from sugarcane bagasse (SCB) included obtaining cellulose after bleaching (CAB), nanocellulose (NC) and then luminescent nanoparticles (LNPs).

The pretreatment procedure was adapted with minor modifications from previously described methods.[10,11] Sugarcane bagasse was cut into small segments (~10 mm), thoroughly washed under running water, and drained. The cleaned material was sun-dried for 1–2 days, then ground and sieved to obtain a fine powder with a particle size of 100 mesh. A portion of 20 g of this powder was boiled in distilled water at a solid-to-liquid ratio of 1:10 (w/v) at 70 °C for 120 minutes to remove water-soluble impurities. The mixture was then filtered, and the solid residue was treated with alkali by refluxing with a 10% NaOH solution (1:10 w/v) at 100 °C for an additional 120 minutes. After filtration, the resulting filtrate was qualitatively tested using concentrated sulfuric acid to assess the presence of lignin. If a precipitate formed, indicating residual lignin, the solid was re-treated with fresh NaOH solution under identical conditions. This process was repeated until no further lignin precipitation was observed. The final residue was thoroughly washed with distilled water to reach a neutral pH.

Bleaching of delignified bagasse

The bleaching process was adapted with modifications from the method reported by Katakojwala and Mohan.[12] The delignified residue was dispersed in a 5% sodium hypochlorite (NaOCl) solution and maintained at 60 °C for 2 hours under constant agitation. After bleaching, the mixture was filtered to separate the solid fraction from the liquid. A successful bleaching process was indicated by the solid residue turning white and the filtrate becoming clear. The resulting cellulose-rich residue was thoroughly washed with distilled water until a neutral pH was achieved. Then, it was subsequently dried in an oven at 60 °C until a constant weight was reached.

Acid hydrolysis of cellulose

The acid hydrolysis procedure was adapted from the method by Fauziyah *et al*.,[13] with slight modifications. A total of 5 grams of bleached cellulose was mixed with 50% sulfuric acid (H_2SO_4) at a solid-to-liquid ratio of 1:20 (w/v). The reaction was carried out at 45 °C for 2 hours under continuous stirring to promote uniform hydrolysis. Following the hydrolysis, the mixture was cooled by adding a fivefold volume excess of distilled water and stirred until homogeneous. The reaction mixture was then neutralized by gradually adding sodium bicarbonate ($NaHCO_3$) until pH stabilization. Centrifugation was performed to separate the pellet, containing nanoscale cellulose fragments, from the supernatant. The resulting pellet was redispersed and ultrasonicated (20–100 kHz) in an ice-water bath until a stable colloidal suspension was formed. The final colloid was stored in a refrigerator at a low temperature before further analysis.

Synthesis of luminescent nanoparticles (LNPs) from nanocellulose

The synthesis of luminescent nanoparticles was conducted by modifying previously reported hydrothermal carbonization methods that utilized cellulosic or biomass-derived precursors, as described in the works of Nair *et al*., Kasinathan *et al*., and Qie *et al*.[14–16] A nanocellulose suspension (4 mL) was first diluted with distilled water at a ratio of 1:20 (v/v), and then transferred into a Teflon-lined stainless steel autoclave. The hydrothermal treatment was conducted at 200 °C for 12 hours. After the reaction was

completed, the autoclave was allowed to cool to room temperature. The resulting product was filtered, and the luminescent nanoparticles were collected in the filtrate. The obtained LNPs were stored in amber glass bottles and refrigerated until further use to preserve their photoluminescent properties.

Characterizations

Characterizations throughout the research were conducted as follows. FT-IR analysis was conducted using a Shimadzu IR Prestige-21, with spectra acquired within the 4000–600 cm^{-1} range, to identify functional groups present in raw bagasse, bleached cellulose, microcrystalline cellulose, nanocellulose, and luminescent particles. The particle size of the obtained nanocellulose was determined using a Horiba Scientific SZ-100 instrument based on the dynamic light scattering (DLS) technique. A Shimadzu UV-Vis spectrophotometer was employed to determine the maximum absorption wavelength of the LNPs, and an Agilent Cary Eclipse fluorescence spectrometer for photoluminescence (PL) spectroscopy was used to examine their fluorescence emission characteristics. These techniques were used to confirm the structural and optical properties of the materials throughout the fabrication process.

Detection of Fe^{3+} ions using luminescent nanoparticles (LNPs)

Luminescent nanoparticles (LNPs) were evaluated for their ability to detect Fe^{3+} ions in aqueous solution. A series of Fe^{3+} solutions with concentrations of 0.1, 1, 10, and 100 µM were prepared by diluting a 0.01 M stock solution. For each test, 3 mL of the LNP suspension was mixed with 1 mL of the corresponding Fe^{3+} solution. The mixtures were stirred thoroughly to ensure they were homogeneous. Photoluminescence (PL) spectroscopy was then performed on each sample to evaluate the optical response of the LNPs to different Fe^{3+} concentrations.

The preparation of luminescent nanoparticles was conducted through a multi-step transformation starting from SCB, followed by sequential chemical treatments to obtain CAB, NC, and finally luminescent LNP via hydrothermal synthesis. The overall fabrication pathway is illustrated in Figure 1, which outlines the key chemical and thermal processes involved in converting biomass-derived cellulose into luminescent carbon-based nanomaterials.

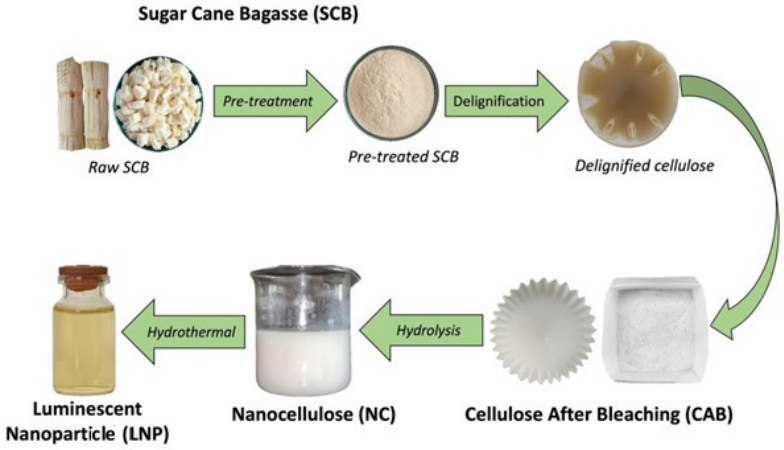

Figure 1: Fabrication steps of luminescent cellulose-based particles – from sugarcane bagasse (SCB), cellulose after bleaching (CAB), nanocellulose (NC) to luminescent nanoparticles (LNPs)

RESULTS AND DISCUSSION

A series of characterizations were performed to evaluate the chemical and optical transformation of sugarcane bagasse into luminescent nanoparticles. Each technique provides complementary information about the materials' composition, size, and functional behavior.

FT-IR spectra analysis

Fourier transform infrared (FT-IR) spectroscopy was conducted to monitor the changes in functional groups throughout the processing stages: from raw sugarcane bagasse to nanocellulose and luminescent nanoparticles. The resulting spectra reflect the progressive removal of non-cellulosic components and the emergence of cellulose-specific features, supporting the chemical refinement during pretreatment and hydrothermal conversion. Figure 2 presents the FT-IR spectra of SCB, CAB, microcrystalline cellulose (MCC), and nanocellulose (NC), illustrating the evolution of the material composition through each processing stage. The SCB spectrum shows a broad O–H stretching band

around 3453 cm^{-1} and a C–H stretching band near 2920 cm^{-1}. A distinct C=O peak at approximately 1735 cm^{-1} is attributed to acetyl and ester groups found in hemicelluloses, whereas the bands between 1600 and 1500 cm^{-1} reflect the aromatic structure of lignin. After bleaching, these signals diminish significantly, indicating a reduction in non-cellulosic components. In the MCC sample, the FT-IR spectrum exhibits more defined peaks, particularly at 1429 cm^{-1} (CH_2 bending) and 897 cm^{-1} (β-glycosidic bonds), suggesting increased structural order and crystallinity.[17] These features persist in the NC sample, which shows firm cellulose-related peaks at 1160 and 1050 cm^{-1}. The broader band observed around 1600–1500 cm^{-1} in the NC may indicate enhanced moisture interaction due to the greater surface area of the material, near 1735 and 1600 cm^{-1}, gradually weakening or disappearing as processing continues, while cellulose-specific peaks, particularly at 1050, 1429, and 897 cm^{-1}, become more prominent.[18] These changes confirm the efficiency of the bleaching and hydrolysis treatments in purifying cellulose and enhancing its crystalline structure.

Table 1 provides a clearer view of the spectral progression across samples. The peaks attributed to lignin and hemicelluloses, such as those at approximately1735 and 1600 cm^{-1}, show a gradual decline in intensity or disappear entirely as the material undergoes successive processing. In contrast, cellulose-related bands at 1050, 1429, and 897 cm^{-1} become increasingly prominent, reflecting the enrichment of cellulose and the development of more ordered structures. These spectral changes highlight the efficiency of the bleaching and hydrolysis steps in removing non-cellulosic constituents and isolating purified cellulose from sugarcane bagasse. The distinct differences observed across the spectra at each treatment stage also underscore the progressive refinement of chemical structure throughout the process.

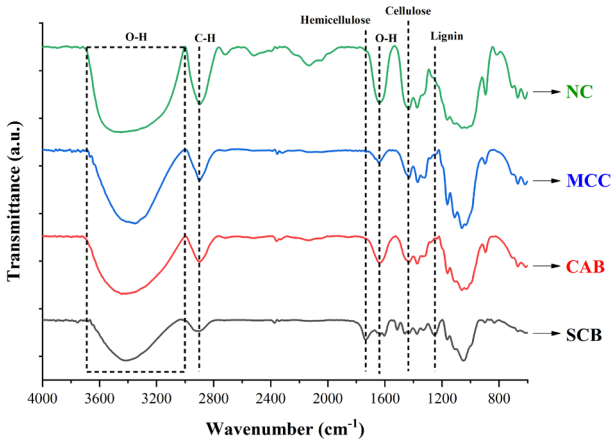

Figure 2: FT-IR spectra of sugarcane bagasse (SCB), cellulose after bleaching (CAB), commercial microcrystalline cellulose (MCC), and nanocellulose (NC)

Table 1
FT-IR absorption bands and their assignments for SCB, CAB, MCC, and NC

Wavenumber (cm^{-1})	Assignment / vibrational mode	Functional group	SCB	CAB	MCC	NC
~3330-3450	O–H stretching	Hydroxyl (–OH)	√	√	√	√
~2920	C–H stretching (asymmetric)	Aliphatic –CH_2	√	√	√	√
~1735	C=O stretching	Ester/acetyl (hemicelluloses)	√	×	×	×
~1600–1505	Aromatic C=C stretching	Lignin	√	↓	×	×
~1425–1430	CH_2 scissoring	Crystalline cellulose	↓	↑	√	√
~1160	C–O–C asymmetric stretching	Cellulose	√	√	√	√
~1050–1030	C–O stretching	Primary/secondary alcohols	√	√	√	√
~895	C1–H deformation, β-glycosidic linkage	Cellulose I structure	↓	↑	√	√↑

Notes: Symbols indicate functional groups of FT-IR peaks across treatments: √ – peak clearly present; ↑ – increased intensity compared to the previous stage; × – peak absent; ↓ – decreased intensity compared to the previous stage

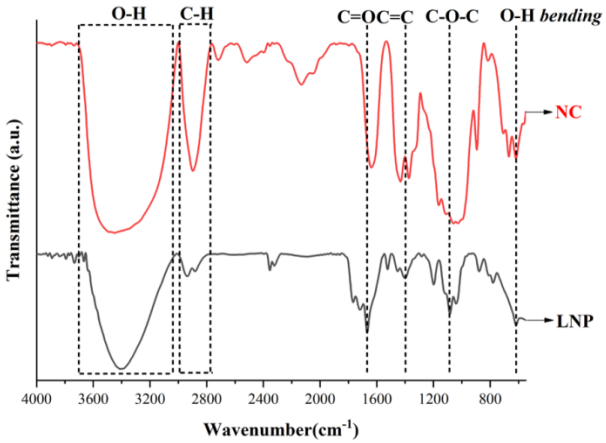

Figure 3: FT-IR spectra of luminescent nanoparticles and nanocellulose

Tabel 2
Summary of FT-IR band assignments of samples at different processing stages

Functional group	Wavenumber (cm^{-1})	Assignment	Observed in
O–H	~3450	Hydrogen-bonded hydroxyl stretching	SCB, CAB, NC, LNP
C–H	~2920	Aliphatic C–H stretching	SCB, CAB
C=O	~1735	Ester/acetyl groups from hemicellulose	SCB
Aromatic C=C	1600–1510	Lignin skeletal vibrations	SCB
CH_2	1429	Bending vibration in cellulose	MCC, NC
C–O–C	1160	Asymmetric stretching in cellulose backbone	MCC, NC, LNP
C–O	1050	Stretching in cellulose	CAB, MCC, NC
β-glycosidic linkage	~897	C1–H deformation, β-configuration	MCC, NC, LNP
C=O / C=C (conjugated)	1700–1600	Aromatized/crosslinked carbonyl structures	LNP

FT-IR spectral comparison of cellulose derivatives and luminescent nanoparticles

The FT-IR spectral comparison between nanocellulose (NC) and luminescent nanoparticles (LNPs), as shown in Figure 3, reveals key structural transformations that correlate with the emergence of photoluminescent properties in LNPs. While NC retains typical cellulose bands, such as O–H stretching (~3340 cm^{-1}), C–O–C vibrations (~1160 cm^{-1}), and β-glycosidic linkages (~897 cm^{-1}), the LNP spectrum displays notable modifications, including the disappearance of the ~1400 cm^{-1} band, which is attributed to CH_2 bending. This suggests cleavage of aliphatic side groups, likely driven by dehydration and partial aromatization during hydrothermal processes. In the LNP spectrum, new absorptions appeared in the 1600–1700 cm^{-1} region, indicative of the formation of carbonyl (C=O) and aromatic (C=C) functionalities, which are crucial to the development of the nanoparticles' luminescent properties.[19]

Table 2 summarizes the FT-IR spectral evolution from raw sugarcane bagasse (SCB) to luminescent nanoparticles (LNPs). Characteristic lignin bands at 1600–1510 cm^{-1} and the hemicellulose-associated carbonyl band near 1735 cm^{-1} were only detected in SCB, confirming effective delignification during pretreatment. Cellulose-specific vibrations, such as C–O–C (1160 cm^{-1}) and β-glycosidic linkages (~897 cm^{-1}), became more prominent in NC and persisted in LNPs, suggesting structural retention of the cellulose backbone.[20] Crucially, the emergence of new bands at 1710 and 1640 cm^{-1} in LNPs indicates oxidation and aromatization during hydrothermal carbonization, which is critical for creating fluorescent centers. The appearance of conjugated C=O/C=C stretches (1700–1600 cm^{-1}) in LNPs indicates carbon core rearrangement and partial aromatization during hydrothermal processing. These structural modifications alter the electronic structure of cellulose, facilitating

excited-state delocalization and the emission of visible light.[21]

Particle size distribution of nanocellulose and derived luminescent nanoparticles

Particle size measurements were performed on nanocellulose (NC) suspensions using dynamic light scattering (DLS). As presented in Table 3 and Figure 4, the NC sample exhibited a Z-average diameter of 165.0 nm with a standard deviation of 62.0 nm, indicating a sub-micron dispersion characteristic of well-dispersed nanocellulose.

This size range aligns with typical nanocellulose dimensions reported in the literature (160–400 nm),[13,14] and suggests that acid hydrolysis using 50% H_2SO_4 for 120 minutes effectively reduced the particle size, without inducing significant aggregation. The colloidal stability observed in the NC suspension is attributed to the surface functionalization by sulphate half-ester groups, which replace hydroxyl moieties during hydrolysis. This substitution enhances interparticle repulsion via electrostatic interactions, thereby minimizing agglomeration and maintaining dispersion uniformity in aqueous media.

Table 3
Z-average diameter and standard deviation of NC and LNPs

Sample	Process parameters	Z-Average (nm)	S.D. (nm)	% of Particles (1–100 nm)
Nanocellulose (NC)	50% H_2SO_4, 120 min	165.0	62.0	~46
Luminescent nanoparticles (LNPs)	200 °C, 12 h (hydrothermal)	192.7	57.3	~38

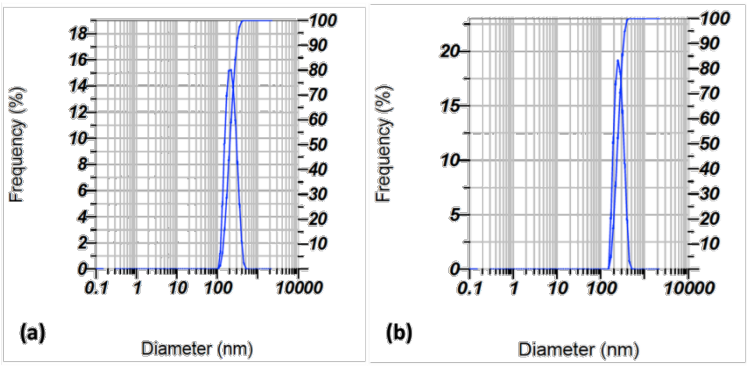

Figure 4: Particle size distribution profiles obtained from DLS-based PSA: (a) nanocellulose (NC), and (b) luminescent nanoparticles (LNPs) – the left Y-axis shows frequency (%), and the right Y-axis indicates cumulative size distribution (%)

The unimodal size distribution shown in Figure 4 (a) further supports the homogeneity of the nanocellulose particles. Following hydrothermal carbonization at 200 °C for 12 hours, the NC was converted into luminescent nanoparticles (LNPs). The resultant LNPs displayed a Z-average diameter of 192.7 nm and a narrower distribution (S.D. = 57.3 nm), as illustrated in Figure 4 (b). The modest increase in size may be attributed to condensation, surface restructuring, or initial graphitization during hydrothermal processes.

This phenomenon indicates a structural reorganization during the conversion of the biomass precursor into carbon dots, possibly leading to the formation of stable colloidal dispersions through surface charge modifications.[22] Despite this increase, the particles remained within the nanoscale domain, indicating that the transformation preserved the colloidal nature of the system. This structural reorganization aligns with proposed mechanisms for carbon dot formation from biomass, where phenolic compounds act as catalytic seeds for growth, and thermally denatured protein components can contribute to nitrogen doping.[23-24] These findings confirm the successful fabrication of luminescent cellulose-based nanoparticles through a sequential hydrolysis and hydrothermal conversion. The

resulting colloids exhibited stable, monodisperse profiles with particle sizes suitable for further application in sensing, photonic, or optoelectronic platforms.

In accordance with the European Commission Recommendation 2011/696/EU and its clarification in the Second Regulatory Review on Nanomaterials (COM/2012/0572 final), the 50% number-based threshold for classifying nanomaterials may be adjusted to 1–50% in cases where functional relevance is significant. As shown in the PSA data (Fig. 4) and summarized in Table 3, although the Z-average diameters exceed 100 nm, approximately 46% of nanocellulose (NC) and 38% of luminescent nanoparticles (LNP) fall within the 1–100 nm range. Considering this substantial nanoscale fraction and the performance-oriented application of the materials, the synthesized products can still be classified as nanomaterials under the EU regulatory framework.[25–26]

UV-Vis absorption analysis of LNPs

The optical absorbance of the luminescent nanoparticles was examined using UV-Vis spectroscopy. Dilution was applied prior to measurement to ensure accurate identification of absorbance peaks. A strong absorption band in the UV region confirms the presence of conjugated carbon structures, consistent with the typical characteristics of carbon-based luminescent materials.

Before measurement, the suspension was diluted to minimize spectral broadening caused by high particle concentration, which often leads to peak overlap and inaccurate absorbance readings. As shown in Figure 5, the UV–Vis spectrum displays two distinct absorption peaks at 221 nm and 284 nm. The peak at 221 nm corresponds to π–π* transitions in C=C bonds, while the more intense band at 284 nm is attributed to n–π* transitions associated with C=O groups on the LNP surface, consistent with previous findings on carbon-based fluorescent nanomaterials.[14] The sharp absorption at 284 nm further supports the presence of conjugated domains and surface-functionalized carbonyl groups, which are critical for the photoluminescent behavior of LNPs.

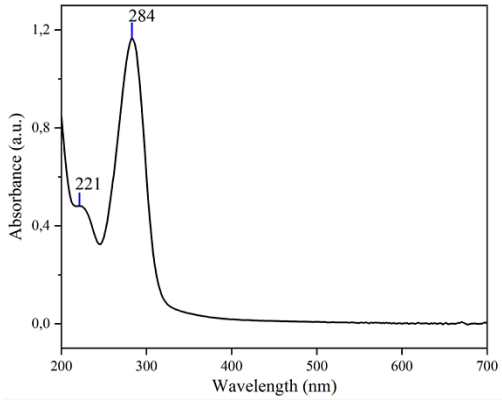

Figure 5: UV–vis absorption spectrum of synthesized LNPs

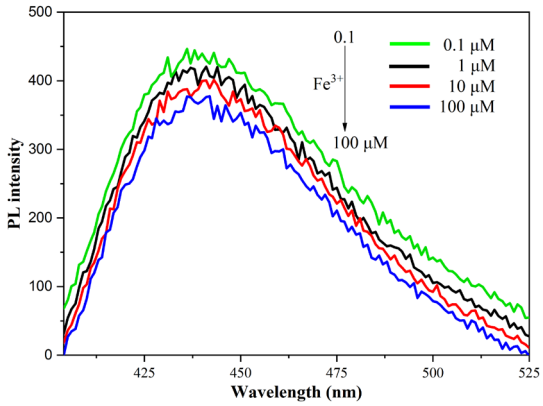

Figure 6: Photoluminescence spectra of LNPs in the presence of Fe^{3+} ions at various concentrations (0.1, 1, 10, and 100 µM)

Application of synthesized LNPs for Fe^{3+} ion detection

Photoluminescence measurements were performed to evaluate the sensing capability of the synthesized LNPs toward Fe^{3+} ions. The photoluminescence (PL) spectra presented in Figure 6 demonstrate the quenching behavior of the synthesized LNPs upon exposure to Fe^{3+} ions at increasing concentrations.

The initial emission intensity, observed around 440-450 nm, gradually decreases as the Fe^{3+} concentration increases from 0.1 to 100 µM. The strongest emission was recorded at 0.1 µM (green line), while the lowest intensity occurred at 100 µM (blue line), indicating a concentration-dependent quenching effect. This decline in PL intensity indicates dynamic quenching, where the excited-state energy of LNPs is non-radiatively dissipated upon interaction with Fe^{3+} ions. Such interactions likely occur through surface binding or electronic energy transfer, suppressing fluorescence emission.

This behavior is consistent with prior reports on carbon dots by Chen *et al.*,[27] where electron

transfer processes between the excited fluorophore and paramagnetic metal ions like Fe^{3+} lead to significant fluorescence quenching. The trend confirms the sensitivity of LNPs toward Fe^{3+} ions and supports its use as an optical probe for detecting trace levels of metal ions in aqueous environments. Given the strong quenching effect, further analysis of the Stern-Volmer constant and quenching mechanism can elucidate the binding affinity and interaction dynamics between the LNPs and Fe^{3+} ions. Furthermore, the selectivity of these carbon dots for Fe^{3+} ions over other metal ions is crucial for practical applications, as demonstrated in similar studies.[27]

CONCLUSION

Luminescent nanoparticles (LNPs) were successfully synthesized from cellulose isolated from sugarcane bagasse through sulfuric acid hydrolysis, followed by hydrothermal carbonization. The LNPs exhibited strong UV absorption at 284 nm and blue fluorescence emission at 445 nm under 360 nm excitation, along with a mean particle size of 192.7 nm and good colloidal stability. Photoluminescence analysis revealed dynamic fluorescence quenching in the presence of Fe^{3+} ions, demonstrating potential for metal ion detection. The novelty of this study lies in the use of cellulose extracted directly from sugarcane bagasse, a low-cost and abundant biomass source, without the need for dopants or surface passivators. This simplified and sustainable approach to nanomaterial synthesis offers a cleaner route for converting agricultural waste into functional luminescent materials suitable for environmental sensing applications. Future work may focus on expanding the sensing applications and integrating the LNPs into portable detection systems for environmental monitoring.

ACKNOWLEDGMENT: The authors gratefully acknowledge the Faculty of Mathematics and Natural Sciences, Universitas Tanjungpura, for the financial support provided through the Year 2024 FMIPA UNTAN Research Grant (Grant No. 2799/UN22.8/PT.01.05/2024).

REFERENCES

[1] O. M. Vanderfleet and E. D. Cranston, *Nat. Rev. Mater.*, **6**, 124 (2021), https://doi.org/10.1038/s41578-020-00239-y

[2] A. A. B. Omran, A. A. B. A. Mohammed, S. M. Sapuan, R. A. Ilyas, M. R. M. Asyraf *et al*., *Polymers*, **13**, 231 (2021), https://doi.org/10.3390/polym13020231

[3] K. Heise, E. Kontturi, Y. Allahverdiyeva, T. Tammelin, M. B. Linder *et al*., *Adv. Mater.*, **33**, 2004349 (2021), https://doi.org/10.1002/adma.202004349

[4] M. Kaur, P. Sharma and S. Kumari, *Int. J. Sci. Res.*, **6**, 1881 (2017), https://doi.org/10.21275/13121701

[5] V. Thakur, A. Guleria, S. Kumar, S. Sharma and K. Singh, *Mater. Adv.*, **2**, 1872 (2021), https://doi.org/10.1039/D1MA00049G

[6] N. M. Marin, *Polymers*, **17**, 1467 (2025), https://doi.org/10.3390/polym17111467

[7] Y. Ma and X. Cheng, *Int. J. Biol. Macromol.*, **253**, 127393 (2023), https://doi.org/10.1016/j.ijbiomac.2023.127393

[8] N. De Acha, C. Elosúa, J. M. Corres and F. J. Arregui, *Sensors*, **19**, 599 (2019), https://doi.org/10.3390/s19030599

[9] W. Zhang, H. Duo, S. Li, Y. An, Z. Liu *et al*., *Colloids Interfaces Commun.*, **38**, 100308 (2020), https://doi.org/10.1016/j.colcom.2020.100308

[10] S. Thiangtham, J. Runt, N. Saito, T. Kondo, Y. Ikeda *et al*., *Cellulose*, **27**, 1367 (2020), https://doi.org/10.1007/s10570-019-02866-3

[11] W. R. Kunusa, R. Abdullah, K. Bilondatu and W. Z. Tulie, *J. Phys.: Conf. Ser.*, **1422**, 012040 (2020), https://doi.org/10.1088/1742-6596/1422/1/012040

[12] R. Katakojwala and S. V. Mohan, *J. Clean. Prod.*, **249**, 119342 (2019), https://doi.org/10.1016/j.jclepro.2019.119342

[13] B. Fauziyah, M. Yuwono and Isnaeni, *Ann. Rom. Soc. Cell Biol.*, **25**, 989 (2021)

[14] S. S. P. Nair, N. Kottam and S. G. P. Kumar, *J. Fluoresc.*, **30**, 357 (2020), https://doi.org/10.1007/s10895-020-02505-2

[15] K. Kasinathan, S. Samayanan, K. Marimuthu and J. H. Yim, *Appl. Surf. Sci.*, **601**, 154266 (2022), https://doi.org/10.1016/j.apsusc.2022.154266

[16] X. Qie, M. Zan, P. Miao, L. Li, Z. Chang *et al*., *J. Mater. Chem. B*, **6**, 3549 (2018), https://doi.org/10.1039/C8TB00193F

[17] D. Trache, A. F. Tarchoun, M. Derradji, T. S. Hamidon, N. Masruchin *et al*., *Front. Chem.*, **8**, 392 (2020), https://doi.org/10.3389/fchem.2020.00392

[18] E. L. da Silva, H. C. Vieira, J. X. dos Santos, C. K. Saul, S. Nisgoski *et al*., *Floresta*, **49**, 411 (2019), https://doi.org/10.5380/rf.v49i3.58864

[19] N. S. Sarma, P. Dutta and S. Chakravarty, in "Dynamics of Advanced Sustainable Nanomaterials and Their Related Nanocomposites at the Bio-Nano Interface", edited by K. Pal and S. Thomas, Elsevier, 2019, pp. 215–233, https://doi.org/10.1016/B978-0-12-819142-2.00009-4

[20] R. Kumar, S. Kumari, S. S. Surah, B. Rai, R. Kumar *et al*., *Mater. Res. Express*, **6**, 105601 (2019), https://doi.org/10.1088/2053-1591/ab3511

[21] E. Espinosa, I. Bascón-Villegas, A. Rosal, F. Pérez-Rodríguez, G. Chinga-Carrasco *et al*., *Int. J. Biol.*

Macromol., **141**, 197 (2019), https://doi.org/10.1016/j.ijbiomac.2019.08.262
[22] E. Lizundia, M. H. Sipponen, L. G. Greca, M. Balakshin, B. L. Tardy *et al*., *Green Chem*., **23**, 6698 (2021), https://doi.org/10.1039/d1gc01684a
[23] K. Lee, E. Park, H. A. Lee, C. Sugnaux, M. Shin *et al*., *Nanoscale*, **9**, 16596 (2017), https://doi.org/10.1039/c7nr04170e
[24] M. Si, M. Sillanpää, S. Zhuo, J. Zhang, M. Liu *et al*., *Ind*. *Crop*. *Prod*., **152**, 112469 (2020), https://doi.org/10.1016/j.indcrop.2020.112469
[25] European Commission, in "Communication from the Commission to the European Parliament, the Council and the European Economic and Social Committee: Second Regulatory Review on Nanomaterials", COM (2012) 572 Final, Brussels, 2012, https://eur-lex.europa.eu/legal-content/EN/TXT/?uri=CELEX:52012DC0572
[26] European Commission, Recommendation on the definition of nanomaterial, *Official Journal of the European Union*, L275/38 (2011), https://eur-lex.europa.eu/eli/reco/2011/696/oj
[27] A. Abbas, T. A. Tabish, S. J. Bull, T. M. Lim and A. N. Phan, *Sci*. *Rep*., **10**, 2162 (2020), https://doi.org/10.1038/s41598-020-78070-2